NASA TECHNICAL NOTE

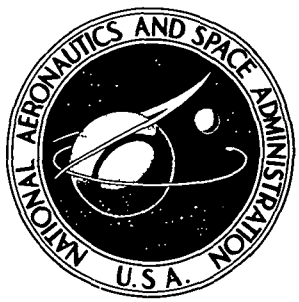

NASA TN D-7273

NASA TN D-7273

FREE-STREAM TEMPERATURE, DENSITY, AND PRESSURE MEASUREMENTS IN AN EXPANSION TUBE FLOW

by Kenneth V. Haggard

Langley Research Center
Hampton, Va. 23665

NATIONAL AERONAUTICS AND SPACE ADMINISTRATION • WASHINGTON, D. C. • OCTOBER 1973

1 Report No	2 Government Accession No	3 Recipient's Catalog No
NASA TN D-7273		

4 Title and Subtitle	5 Report Date
FREE-STREAM TEMPERATURE, DENSITY, AND PRESSURE MEASUREMENTS IN AN EXPANSION TUBE FLOW	October 1973
	6 Performing Organization Code
7 Author(s)	8 Performing Organization Report No
Kenneth V. Haggard	L-8788
	10 Work Unit No
9 Performing Organization Name and Address	502-27-01-03
NASA Langley Research Center Hampton, Va. 23665	11 Contract or Grant No
	13 Type of Report and Period Covered
12 Sponsoring Agency Name and Address	Technical Note
National Aeronautics and Space Administration Washington, D.C. 20546	14 Sponsoring Agency Code

15 Supplementary Notes

16 Abstract

An experimental study has been conducted to determine test-flow conditions in the Langley pilot model expansion tube. Measurements of temperature, density, wall pressure, pitot pressure, and shock and interface velocities have been compared with theoretical calculations based on various models of the flow cycle. The vibrational temperature and integrated density of the molecular oxygen component of the flow were measured by use of vacuum ultraviolet absorption techniques. These measurements indicate both the presence and possible degree of nonequilibrium in the flow. Data are compared with several simplified models of the flow cycle, and data trends are discussed.

17 Key Words (Suggested by Author(s))	18 Distribution Statement
Expansion tube Vibrational temperatures	Unclassified – Unlimited

19 Security Classif. (of this report)	20 Security Classif (of this page)	21 No of Pages	22 Price*
Unclassified	Unclassified	51	Domestic, $3.50 Foreign, $6.00

*For sale by the National Technical Information Service, Springfield, Virginia 22151

FREE-STREAM TEMPERATURE, DENSITY, AND PRESSURE MEASUREMENTS IN AN EXPANSION TUBE FLOW

By Kenneth V. Haggard
Langley Research Center

SUMMARY

An experimental study has been conducted to determine test-flow conditions in the Langley pilot model expansion tube. Measurements of temperature, density, wall pressure, pitot pressure, and shock and interface velocities have been compared with theoretical calculations based on various models of the flow cycle. The vibrational temperature and integrated density of the molecular oxygen component of the flow were measured by use of vacuum ultraviolet absorption techniques. These measurements indicate both the presence and possible degree of nonequilibrium in the flow. Data are compared with several simplified models of the flow cycle, and data trends are discussed.

INTRODUCTION

The Langley pilot model expansion tube is a ground based facility capable of producing a short-duration flow with a velocity, density, and temperature which simulate the conditions encountered by an entry vehicle. The method used to produce the test flow not only can be used with a variety of test gases but also avoids the creation of the high-enthalpy stagnation region present in most other entry simulation devices. The elimination of the stagnation region reduces the effects of chemical and thermal nonequilibrium on the flow cycle.

Previous experimental studies of expansion tube flows (refs. 1 and 2) have shown that the wall pressure and pitot pressure in the test flow are significantly different than those theoretically predicted. Although the importance of nonequilibrium effects is reduced in a facility of this type, its effects can alter the test condition. Thus, the present study was undertaken to characterize the degree of nonequilibrium in the flow by measuring the vibrational temperature of the test flow in the Langley pilot model expansion tube. The experimental method used the well-known vacuum ultraviolet absorption properties of the oxygen molecule and constituted a measurement of the vibrational temperature of the oxygen molecule. Integrated oxygen densities along the absorption path are

V	velocity, m/s
V_i	velocity of secondary interface, m/s
$V_{S,1}$	velocity of primary shock, m/s
x	distance along tube, m
Z	compressibility factor, $p/\rho RT$
$\alpha = \frac{A_{147}}{A_{160}}$	(see eq. (4))
γ	isentropic exponent
$\Delta = \frac{p_{t,c}}{p_t}$	(see eq. (9))
λ	wavelength, nm
ρ	density, kg/m^3
ρ_d	scale depth, cm (see eq. (6))
ρ_{O_2}	density of O_2, kg/m^3

Subscripts:

0	standard conditions
1	initial state in intermediate chamber
2	state behind primary shock
5	state of test-gas flow
10	initial state in acceleration chamber

These flow models neglect the effects of diaphragm losses, viscosity, extraneous shock waves, and finite chemical and vibrational relaxation rates. References 3, 4, and 5 give calculated performance curves based on these models. The effects of finite chemical and vibrational relaxation rates have been considered in references 6, 7, and 8. The flow model used in these reports was inviscid, free of reflected shocks, and assumed equilibrium behind the primary shock, while the chemical model contained only N_2, O_2, N, and O. These restrictions and the uncertainty in the values of the chemical and vibrational relaxation rates limit the use of these calculations to providing a qualitative feel for the processes being studied. These nonequilibrium models, though simplified, do suggest that for the temperature and density ranges of concern in expansion-tube flows, the chemistry will depart from equilibrium in the test flow because of the rapid cooling in the expansion fan.

Calculation of the test-flow conditions has frequently been based on the flow cycle of figure 1(a). For a primary shock wave of a given strength, the state in region 2 is determined from the Rankine-Hugoniot relations on the assumption of local thermodynamic equilibrium. An unsteady expansion at constant entropy then yields the velocity of the test flow as a function of pressure or any thermodynamic state property.

It would be desirable for comparison with the present results if finite relaxation rates were included in the calculations so that nonequilibrium effects could be predicted. The only nonequilibrium calculation method available is that of references 6, 7, and 8. However, because of the limited utility of this program and the necessity to perform a separate calculation for each streamline, no finite-rate calculations were performed in the present study. Instead, a limiting situation of zero-relaxation rate (frozen flow) was calculated, in which the composition and vibrational energy are assumed to remain constant through the expansion at the equilibrium condition established behind the primary shock wave. This calculation takes the form of a "perfect-gas" isentropic expansion of a mixture of atoms ($\gamma = 5/3$) and diatomic molecules ($\gamma = 7/5$). The isentropic exponent of the mixture may be computed from the compressibility factor in state 2 behind the primary shock by the relation

$$\gamma_2 = \frac{4 + 3Z_2}{4 + Z_2} \tag{1}$$

A different calculation method is to incorporate the effects of the reflected shock at the secondary diaphragm location. However, the flow situation sketched in figure 1(b) shows that the reflected shock varies in strength for the different stream paths, depending on the extent to which it has been weakened by interaction with the expansion fan,

The stations at which p_w and p_t were measured were located just upstream and just downstream of the ultraviolet beam. Time correlations between these various measurements were made by using the measured interface velocity.

DATA REDUCTION

The vibrational temperature and density of O_2 were determined from the absorption measurements by using the method of references 11 and 12. Basic data and a theoretical treatment are found in references 13 and 14. With this technique the absorptivity of the flow is measured at two wavelengths. These wavelengths are selected so that the absorption coefficient at one is very sensitive to temperature whereas the absorption coefficient at the other is relatively insensitive to temperature. The degree of absorptivity is also controlled by the density of O_2 in the flow. Thus, since the absorption coefficients are functions of only temperature and wavelength, the temperature is easily determined. This procedure will become clear by considering the equations governing the absorption process.

The absorption of the ultraviolet radiation was assumed to follow Beer's law. Thus,

$$I_\lambda(t) = I_{\lambda,o}(t)\exp\left[-\frac{1}{\rho_0}\int \rho(t)k_\lambda(t)\,d\ell\right] \tag{2}$$

where ρ is the absorber density and the integral is taken over the absorption path. The parameter A_λ at λ is

$$A_\lambda(t) = \log_e\left[\frac{I_{\lambda,o}(t)}{I_\lambda(t)}\right] = \int \frac{\rho(t)k_\lambda(t)}{\rho_0}\,d\ell \tag{3}$$

and the ratio of A_{147} and A_{160} is defined by

$$\alpha(t) = \frac{A_{147}(t)}{A_{160}(t)} = \frac{\int \rho(t)k_{147}(t)\,d\ell}{\int \rho(t)k_{160}(t)\,d\ell} \tag{4}$$

where subscripts 147 and 160 represent values of λ.

The data-reduction model for density and T_{v,O_2} includes the following assumptions:

The result of this procedure is shown by the band in figure 5. The width of the band indicates the probable error in the average. The results of applying this averaging process to a series of different nominal conditions are shown in figure 6.

Aside from the initial acceleration of the interface, there is no clear trend to indicate any systematic change of the velocity as the interface moves down the tube. The lack of a pronounced deceleration is in disagreement with the results of reference 1. These previous results are shown in figure 7. These data show a definite overshoot occurring 1.2 meters downstream of the secondary diaphragm, and the severity of the overshoot increases with increasing p_{10}. An examination of the equipment and data-reduction procedure has not shown any reason for this discrepancy. The variation of the tube diameter was checked to determine whether significant variations in the length of the standing wave could occur, and it was found that they could not. Even if such a pattern had been found, it would not account for the observed dependence on p_{10}. Different tube sections were used for these tests, but again it is not understood how this could produce such an effect. In view of the uniform V_i measured during this study, no attempt has been made to use the interface attenuation model described in reference 1.

The measurement of V_i was standardized by using the value obtained from the microwave technique over the last 1.6 meters of the tube. This measurement agreed to within 1 percent with the value obtained from pressure and phototube measurements along the tube.

Density Parameter

The absorption technique yields a measurement of the integrated density of O_2 along the absorption path. This O_2 density can be related to a total density but this relationship requires the use of assumptions about the structure of the test "slug." Rather than imposing these restrictions the density will be expressed in the parameter ρ_d. The total density is then obtained by using

$$\rho = \frac{\rho_{O_{2,0}} \rho_d}{lF} \tag{7}$$

This equation requires the choice of an l that corresponds to an effective flow diameter; and the mass fraction F of O_2 in the flow. The range of proper values for l and F will become apparent when the data trends are examined.

It is now possible to estimate the pitot pressure based on this density and the measured interface velocity. Thus,

$$p_{t,c} = \frac{\rho_{O_{2,0}} \rho_d}{DF} V_i^2 \tag{8}$$

For these initial conditions the pitot pressure drops sharply, or dips, during the test flow. One objective of this study was to obtain more complete data for the dip condition to aid in explaining this phenomenon.

Measurements during this dip condition are shown in figure 9; initial conditions are listed in table 1. Pitot pressure p_t starts well below the ISFE prediction and increases for about 100 microseconds. (See fig. 9(a).) During the period between 40 and 165 microseconds, p_t lies between the ISEE and ISFE calculations. A sudden drop in p_t ends this period of "uniform" flow. After the dip occurs, the pressure record becomes very spiked but it is clear that the dip lasts about 100 microseconds. Scale depth ρ_d (fig. 9(b)) shows the same general trend as p_t. Values first increase to a reasonably steady level and then decrease. This decrease starts earlier and is slower than that for p_t. This difference is thought to be caused by the integrating effects of the ρ_d measurement. It is interesting to note that in the p_t dip, p_t is reduced by about 50 percent, roughly the same percentage as occurs in ρ_d. This agreement implies that the pitot pressure dip is a direct result of density decrease in the flow. Values of T_{v,O_2} (fig. 9(c)) start near the values of the ISFE calculation, fluctuate a bit, and then decrease slowly for about 40 microseconds. The temperature remains uniform with only minor, short-lived deviations for the rest of the test time. These deviations probably result from the data-reduction technique rather than from real changes in T_{v,O_2}. Changes in Δ (fig. 9(d)) are noticeably different for this example. There is a general increase, lasting 40 microseconds, followed by a uniform level at 1.5 ± 8 percent, much larger than the 0.8 value in the first example. The sudden changes that occur at the time of the dip probably indicate a breakdown in the assumption of uniformity in the radial direction.

Data Trends

As a means of obtaining data trends, tests have been grouped according to test gas composition, p_1 and $V_{S,1}$. The results of each group were then plotted as a function of V_i. Since the primary diaphragm was pressure burst, the scatter in driver pressure caused a small random variation in $V_{S,1}$. In order to correct for this variation, all data for the same nominal conditions behind the primary shock were standardized to an average $V_{S,1}$ and the data were corrected accordingly. Thus, a measured value Y (pressure or temperature) was corrected by using the relation

$$\left(\frac{Y_{ISEE} - Y_{corr}}{Y_{ISEE} - Y_{ISFE}}\right)_{V_{s,s}} = \left(\frac{Y_{ISEE} - Y_{meas}}{Y_{ISEE} - Y_{ISFE}}\right)_{V_{s,m}} \tag{10}$$

78 percent N_2 mixture at the initial conditions of example 1 are shown in figure 13. These data were generated from a computer program originated by C. J. Schexnayder and J. S. Evans of the Langley Research Center. This program solves for the flow behind a normal shock. It allows chemical nonequilibrium but does assume vibrational equilibrium. In figure 13 the abscissa is the time of entrance of the particle path into the expansion fan and the ordinate is the ratio E of chemical energy tied up in dissociation to the corresponding value for equilibrium conditions. Thus, if equilibrium is to be attained, this ratio must be unity. That part of the flow that will form the test slug enters the fan during the first 30 microseconds. Consequently, according to this calculation the flow in region 2 should be considered to be out of equilibrium, and nonequilibrium-flow calculations for this type of expansion tube should start at the primary shock – not at the secondary interface as in references 6, 7, and 8.

It should be noted that, because of the nature of the expansion-tube flow cycle, a significantly lower level of dissociative nonequilibrium is achieved than in a steady flow nozzle for the same test condition. The expansion tube avoids the high enthalpy state of a stagnation reservoir, so that the peak temperatures produced in such a reservoir are reduced. Some perspective of the present level of dissociation is obtained by comparing the highest value of the compressibility factor Z in the present study (corresponding to equilibrium behind the primary shock), which is less than 1.04, with the equilibrium value of 1.45 which would occur behind a bow shock on a model for this test condition.

A summary of Δ is shown in figure 14; Δ was defined as

$$\Delta = \frac{\rho_{O_{2,0}} \rho_d V_i^2}{DFp_t} \tag{11}$$

Several assumptions are included in this definition and the breakdown of these assumptions will cause this parameter to be different from unity. For example F has been assumed to be F_2, but according to the results detailed in figure 13, F should be closer to F_1 (about 15 percent larger for the average run). Variations of V_5 with time are also important, but the largest error is probably caused by a nonuniform radial distribution of temperature, density, and flow velocity.

The method of illustrating trends in Δ in figure 14 is different from that used for other variables. The early value is still indicated by the base of the arrow, but the head of the arrow is replaced by the symbol and gives the value of Δ 75 microseconds back in the flow. In all cases Δ had reached a steady value ($\pm$10 percent) by this time and this value represents the test core value.

It may help to remember the manner in which the test conditions vary with interface velocity; that is, for the same conditions behind the primary shock, expansions to higher

The wall pressure and pitot pressure measurements, in accord with those obtained in previous studies in this facility, approximated the value calculated by the incident-shock, frozen-expansion model or fell between this value and the incident-shock, equilibrium-expansion calculation. None of the measurements suggested that any improvement in the calculation flow model was achieved by including the effects of a reflected or standing shock at the secondary diaphragm. The wall pressure, pitot pressure, and temperature measurements indicate that the simplest reasonably accurate prediction of test gas state would neglect any shock reflection at the secondary diaphragm and use the mean of the equilibrium and frozen expansion models.

Density measurements at conditions for which the pitot-pressure dip occurs indicate that the pitot pressure decrease is principally the result of a density decrease.

The path integrated density measurements at conditions free from the pitot-pressure dip are, of course, influenced by the wall boundary layer. The results of calculations show that these densities can be brought into agreement with the measured pitot pressure and interface velocity by assuming that the boundary layer accounts for a 20-percent decrease in the effective path length.

Langley Research Center,
National Aeronautics and Space Administration,
Hampton, Va., June 12, 1973.

The error in α from the relation

$$\alpha = \frac{A_{147}}{A_{160}}$$

becomes

$$\Delta\alpha = \left[\left(\frac{\partial\alpha}{\partial A_{147}}\right)^2 (\Delta A_{147})^2 + \left(\frac{\partial\alpha}{\partial A_{160}}\right)^2 (\Delta A_{160})^2\right]^{1/2}$$

$$= \left[\left(\frac{\Delta A_{147}}{A_{160}}\right)^2 + \left(\frac{A_{147}}{A_{160}}\right)^2 \left(\frac{\Delta A_{160}}{A_{160}}\right)^2\right]^{1/2}$$

This $\Delta\alpha$ was used with the data of figure 4 to calculate the error involved in measuring T_{v,O_2} by assuming a 1-percent error in the measurements of $I_{\lambda,o}$ and I_λ for each wavelength. The results of these calculations are shown in figure 16. The data covered in this study fall in the range $2 < \rho_d < 12$.

12. Anderson, Olof L.: An Experimental Method for Measuring the Flow Properties of Air Under Equilibrium and Non-Equilibrium Flow Conditions. The High Temperature Aspects of Hypersonic Flow, Wilbur C. Nelson, ed., AGARDograph 68, Pergamon Press, 1964, pp. 299-313.

13. Evans, John S.; and Schexnayder, Charles J., Jr.: An Investigation of the Effect of High Temperature on the Schumann-Runge Ultraviolet Absorption Continuum of Oxygen. NASA TR R-92, 1961.

14. Herzberg, Gerhard: Molecular Spectra and Molecular Structure. I. Spectra of Diatomic Molecules. Second ed., D. Van Nostrand Co., Inc., c.1950. (Reprinted Feb. 1963.)

15. Friesen, Wilfred J.: Use of Photoionization in Measuring Velocity Profile of Free-Stream Flow in Langley Pilot Model Expansion Tube. NASA TN D-4936, 1968.

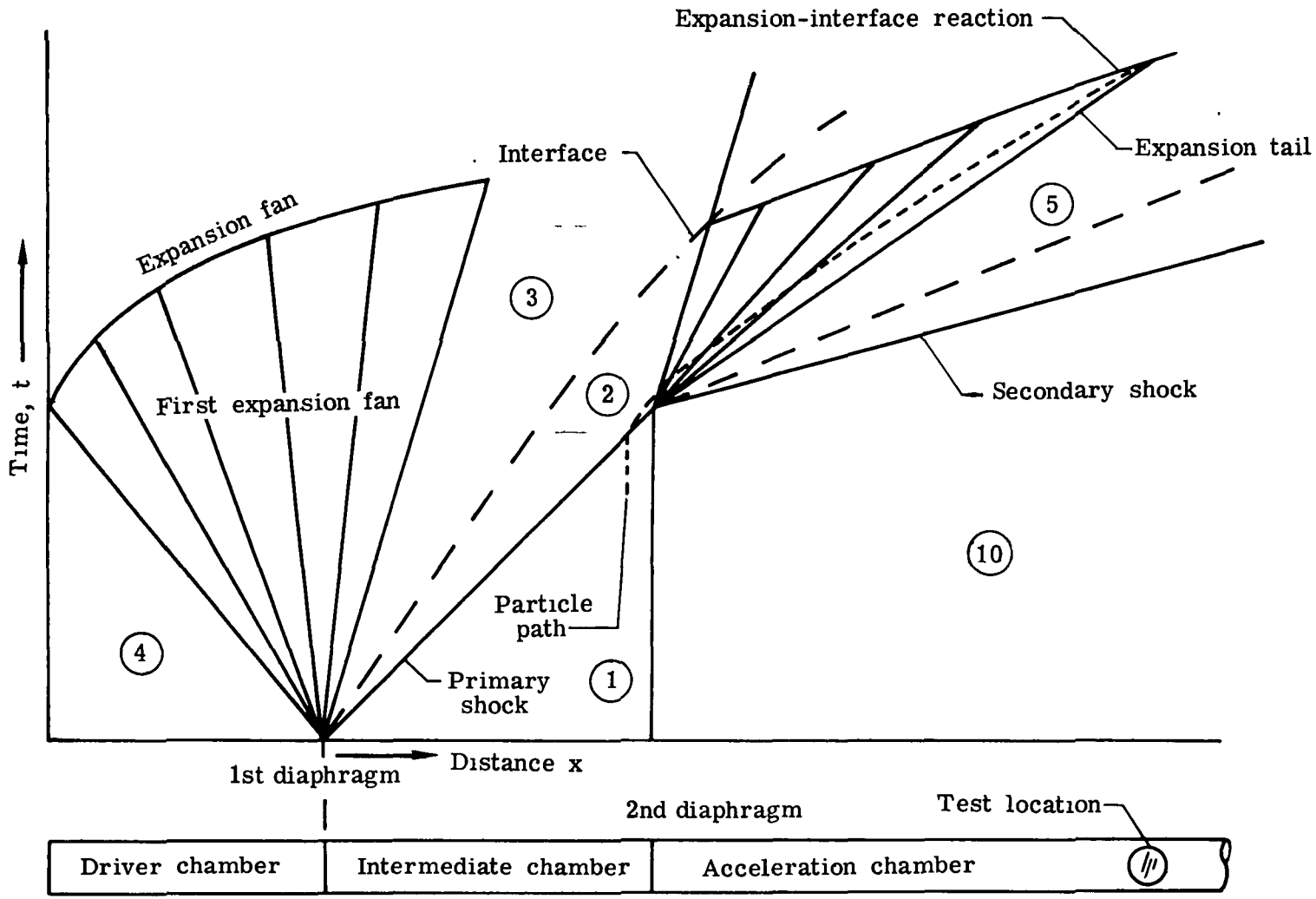

(a) Expansion-tube flow cycle showing pertinent flow regions.

Figure 1.- Distance-time diagrams.

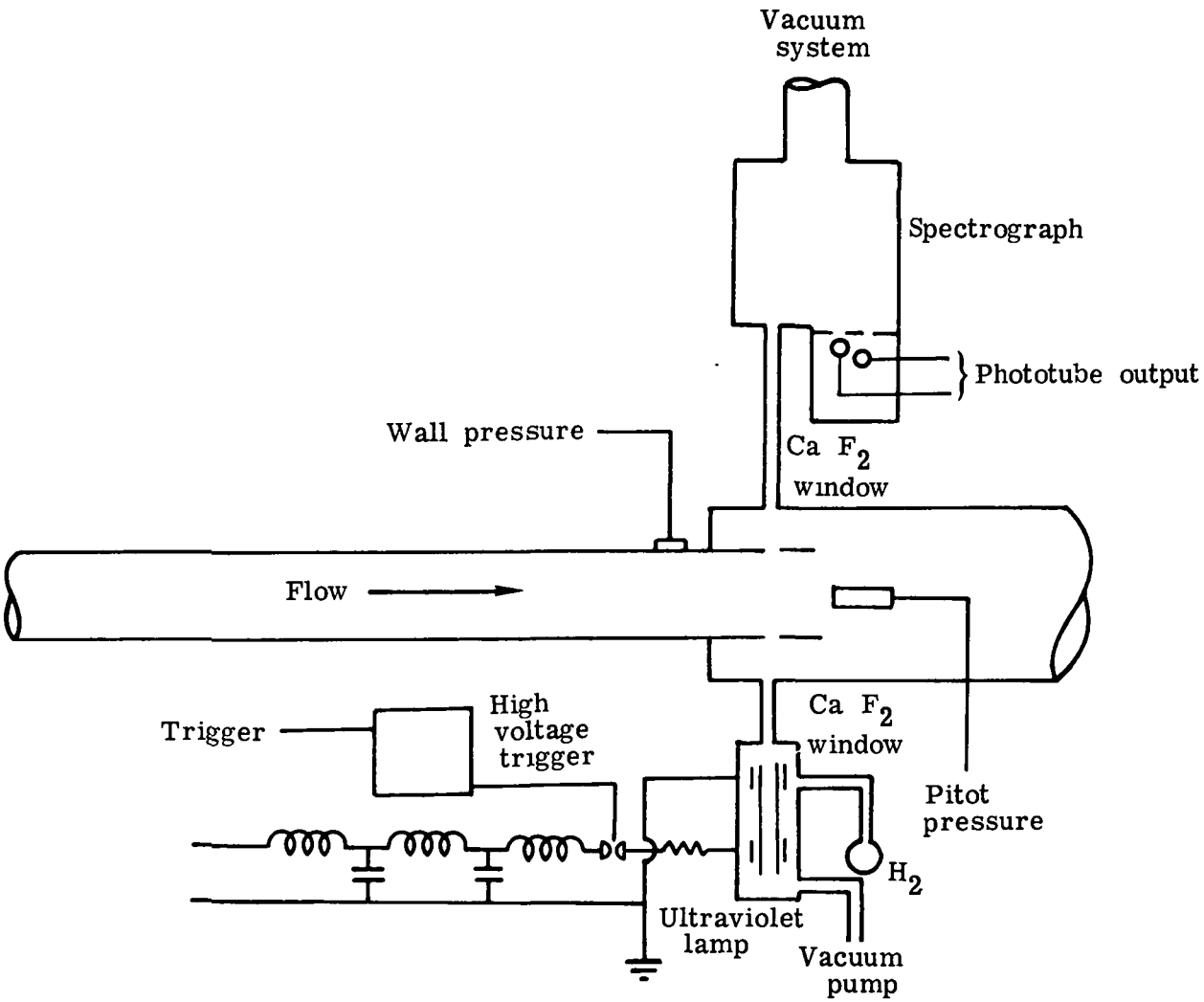

Figure 2.- Sketch of test section and lamp assembly.

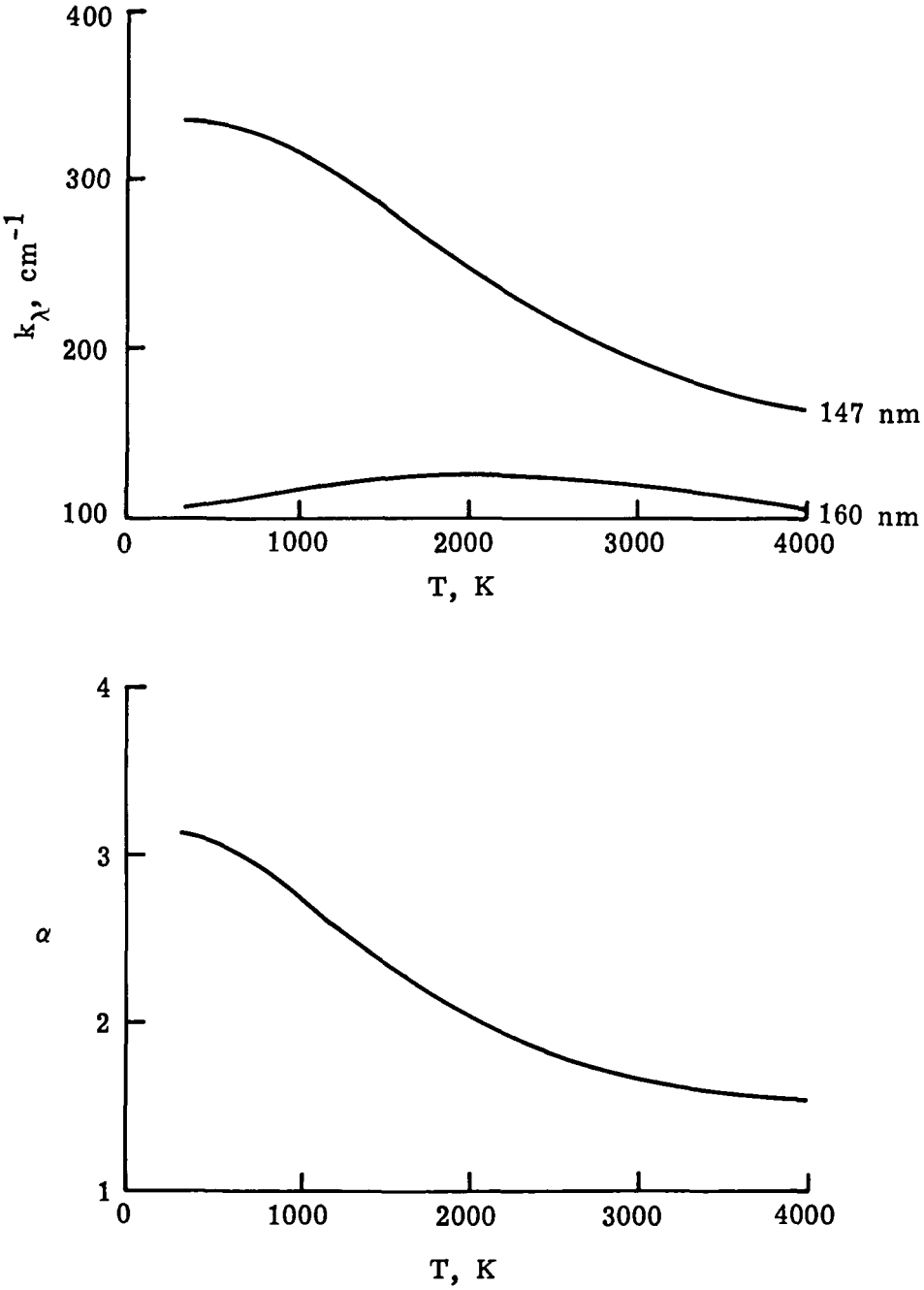

Figure 4.- Temperature dependence of absorption coefficients and their ratio (from ref. 10).

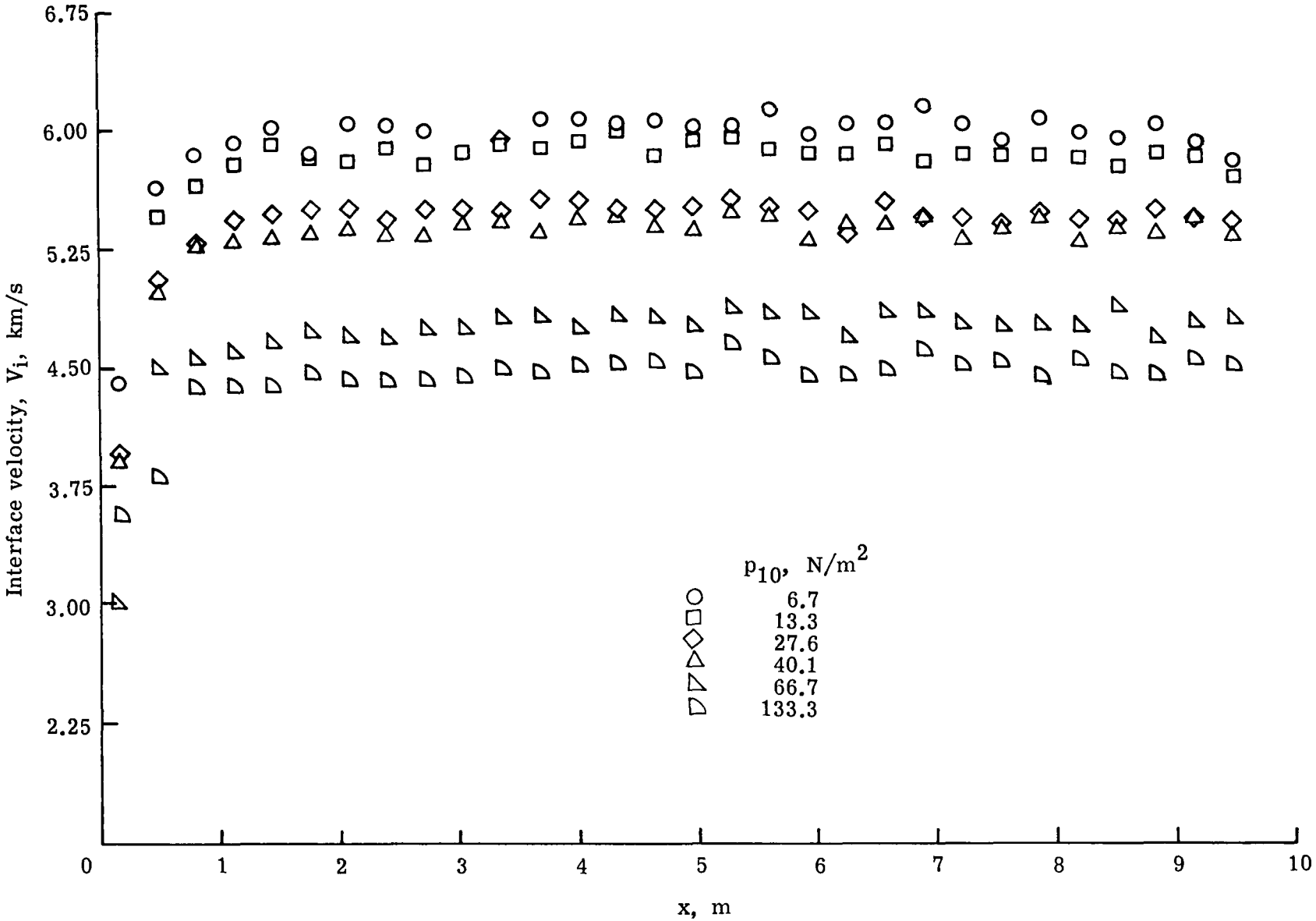

Figure 6.- Interface velocities as determined by microwave measurements.

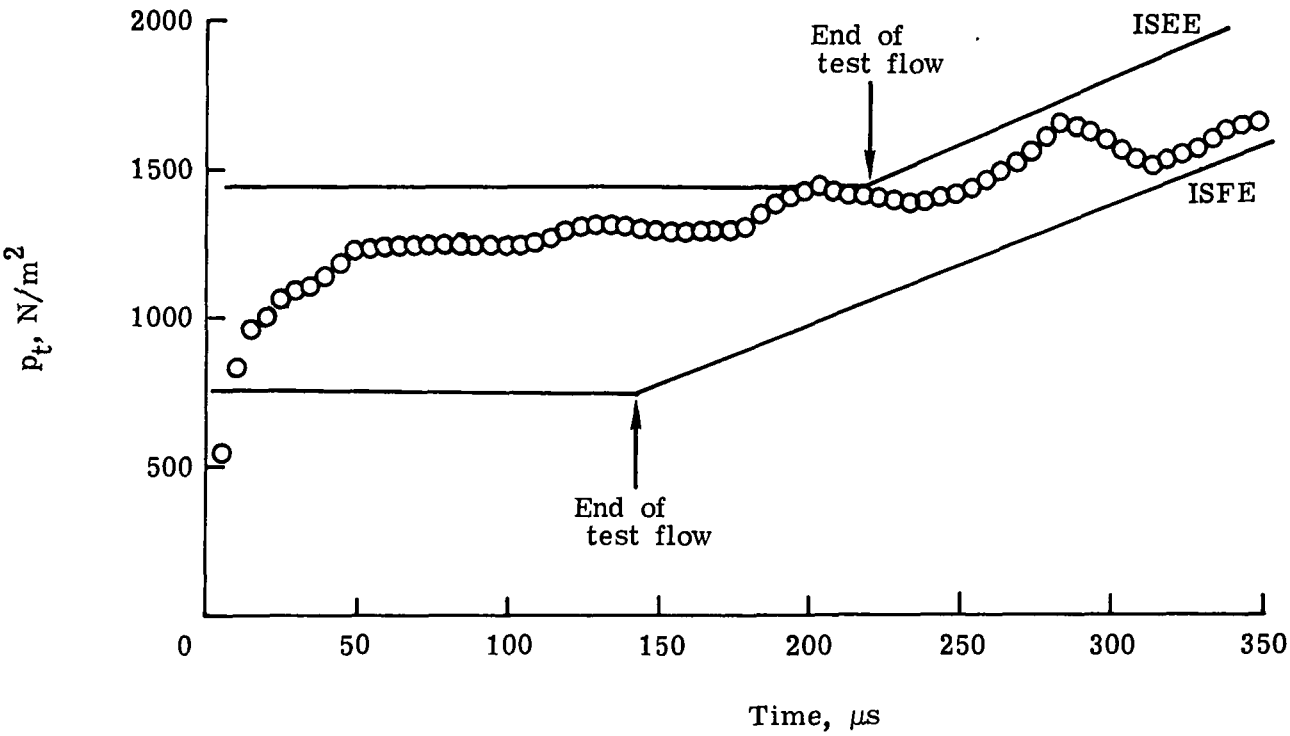

(a) Time history of p_t.

Figure 8.- Example of typical test results.

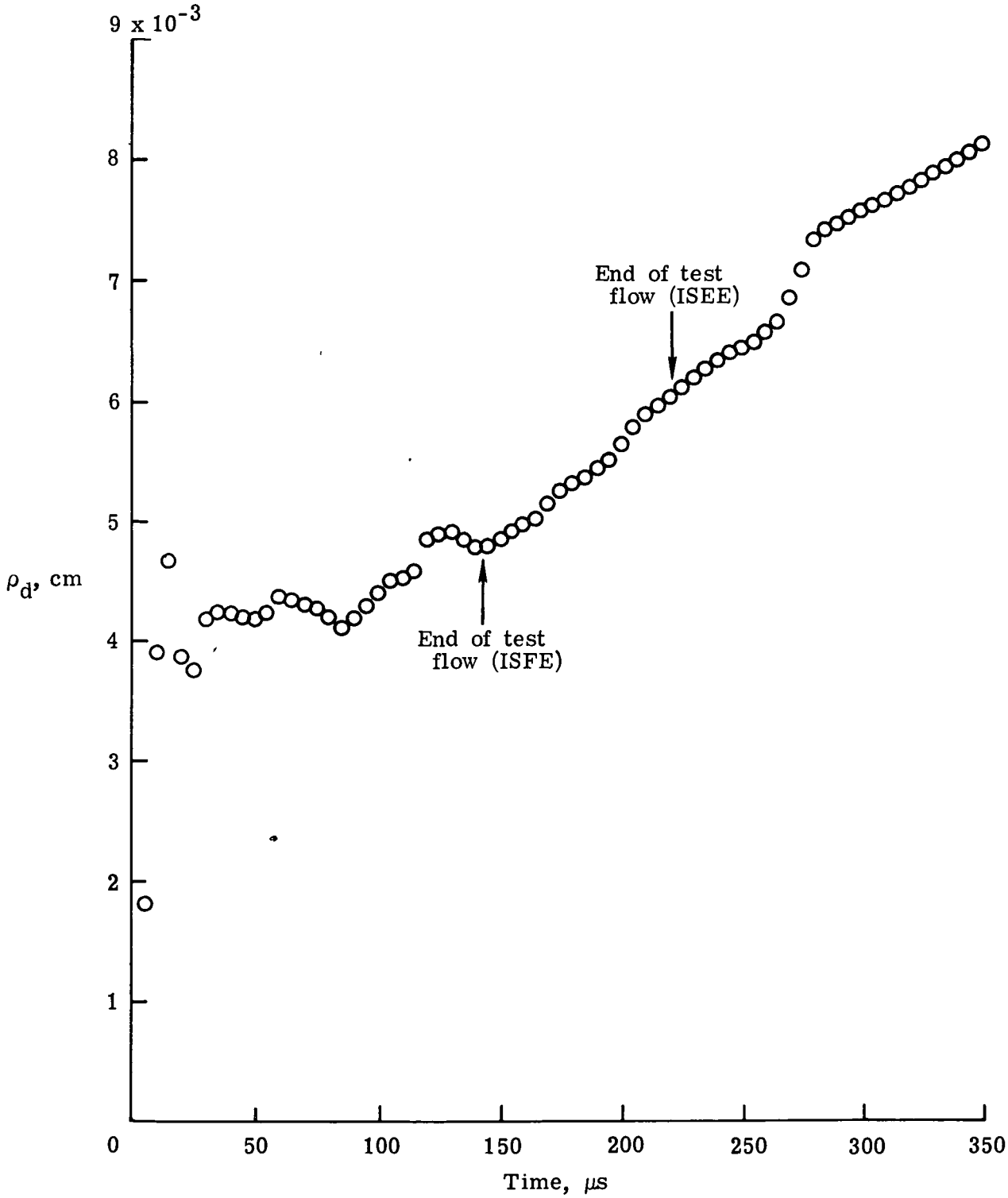

(c) Time history of ρ_d.

Figure 8.- Continued.

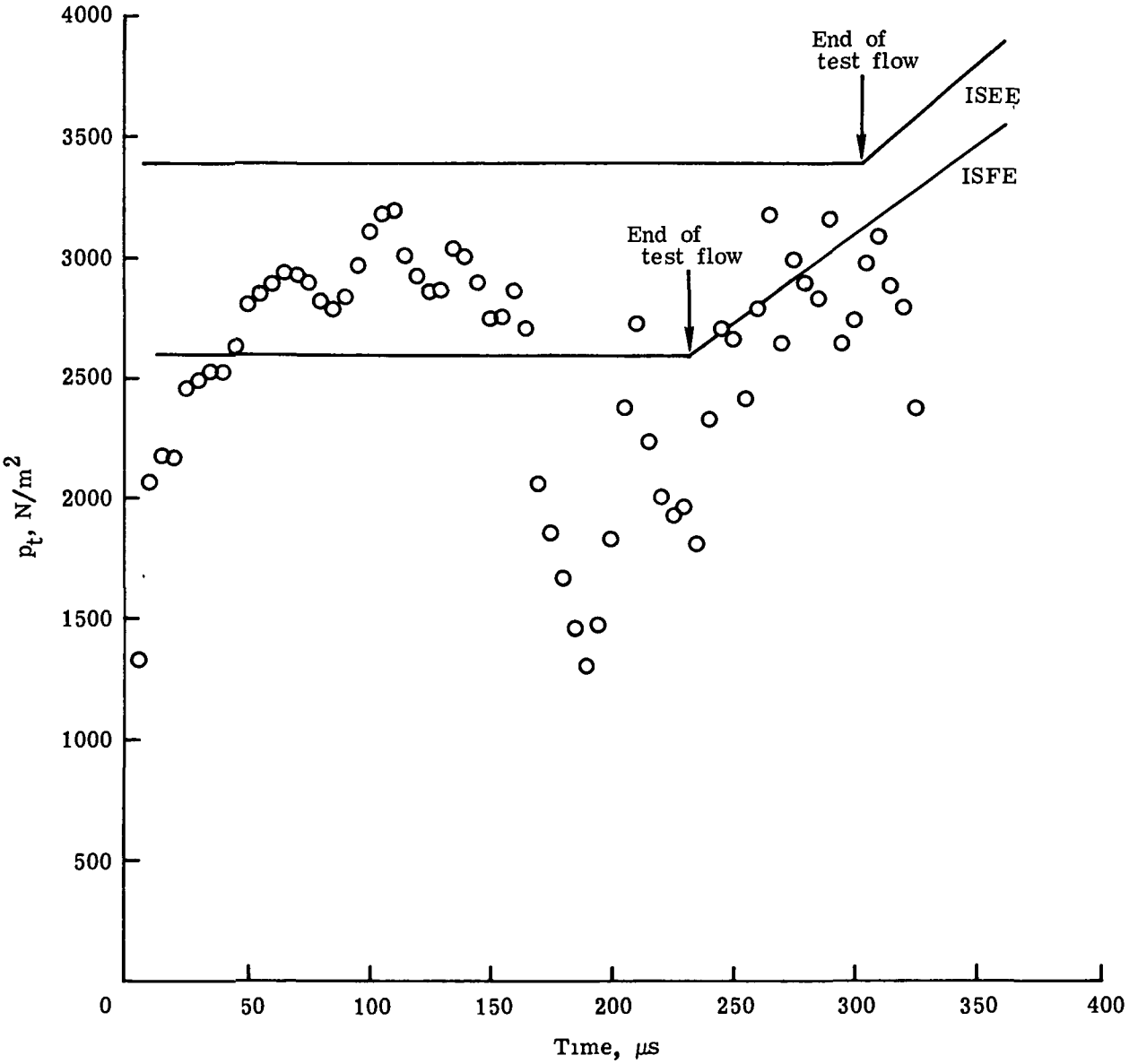

(a) Time history of p_t.

Figure 9.- Example of typical test results at the pitot pressure dip condition.

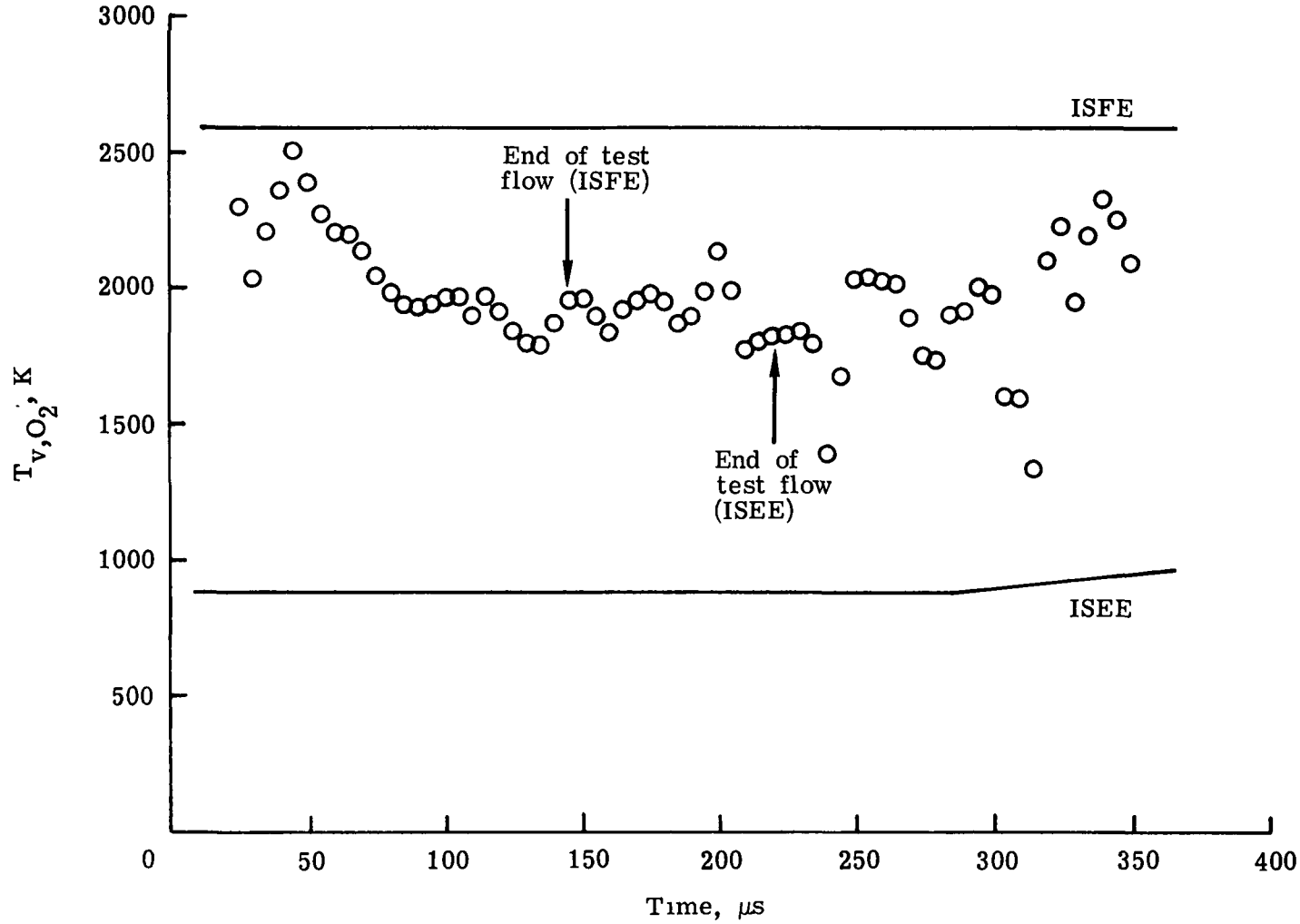

(c) Time history of T_{v,O_2}.

Figure 9.- Continued.

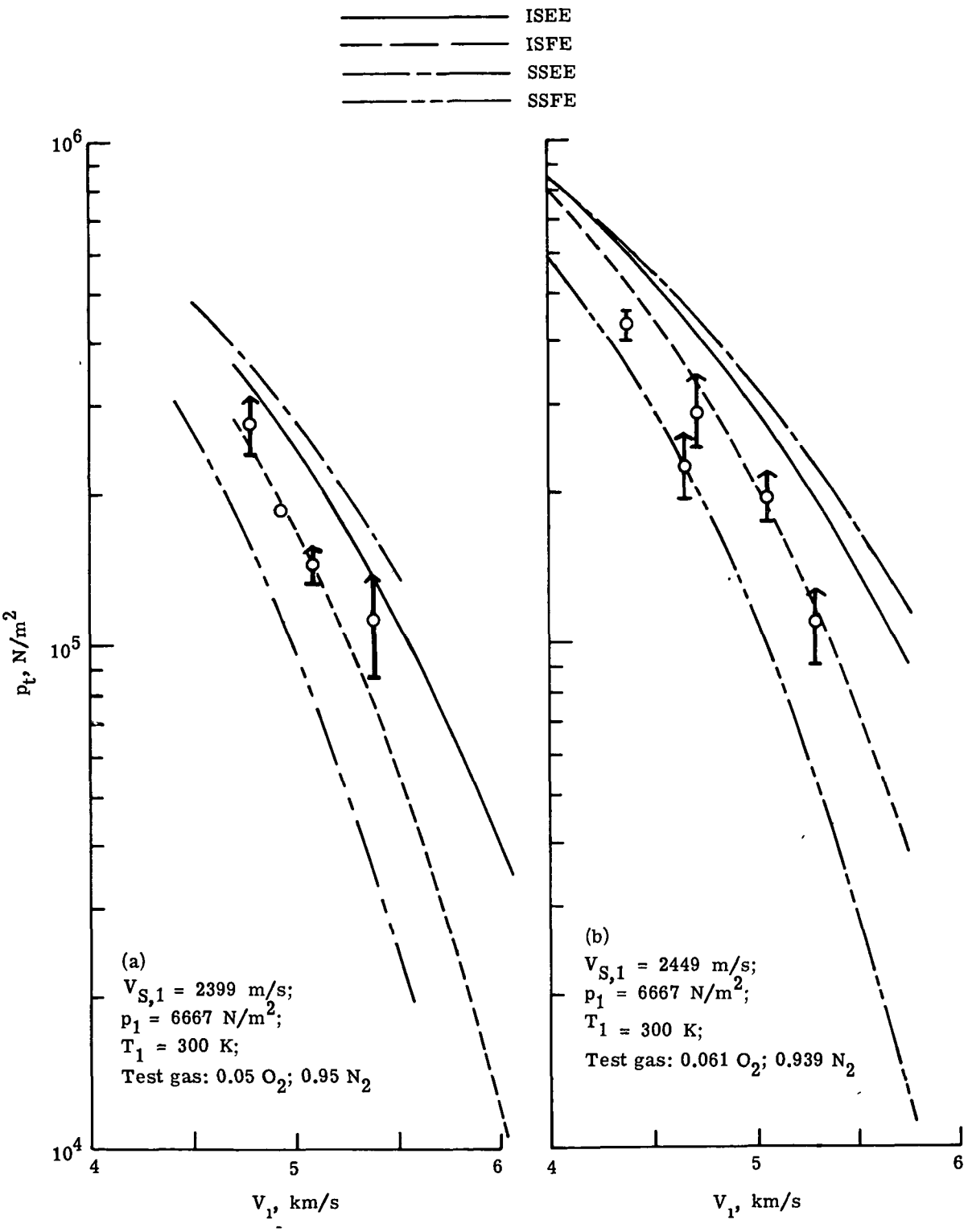

Figure 10.- Comparison of measured and calculated pitot pressure.

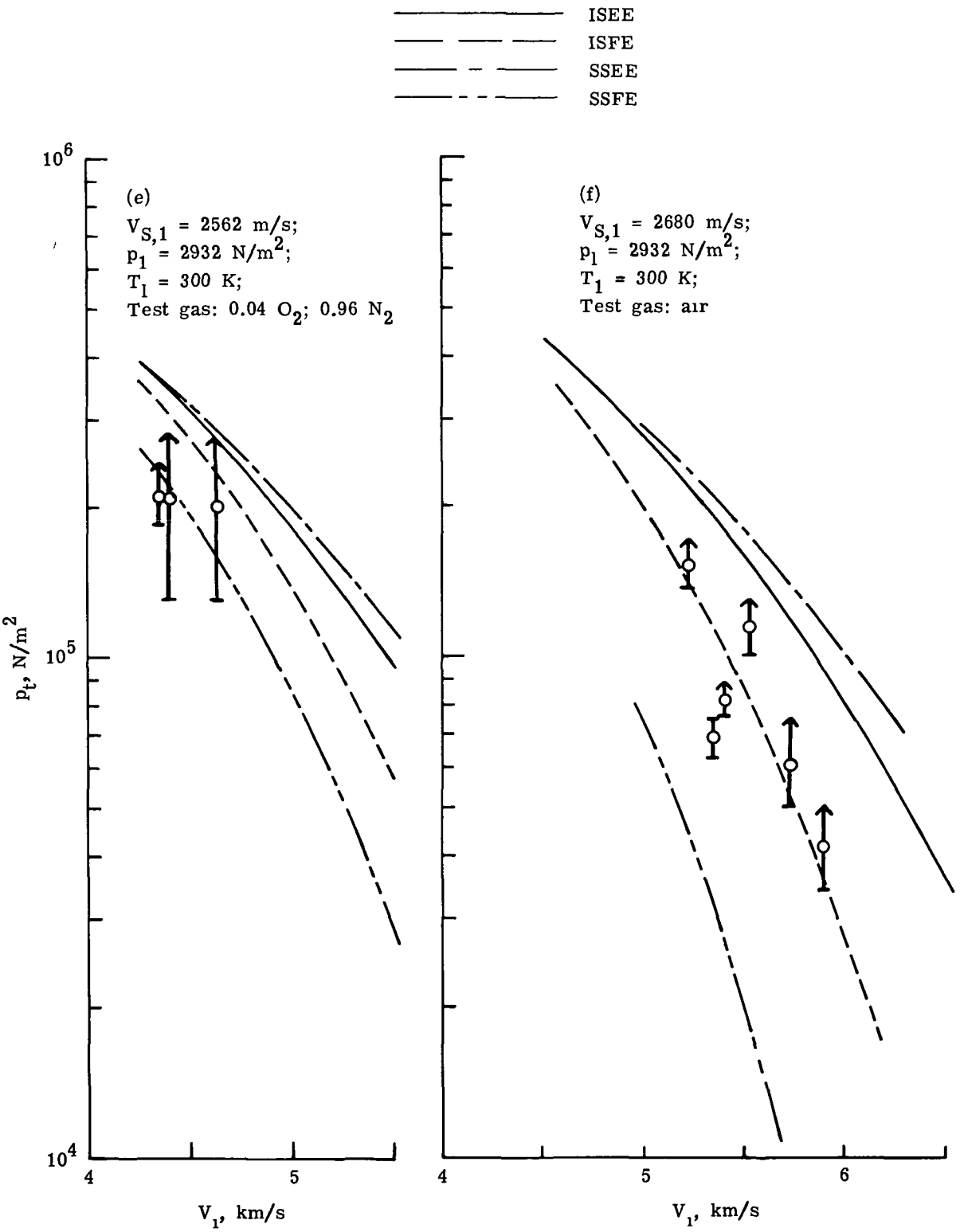

Figure 10.- Continued.

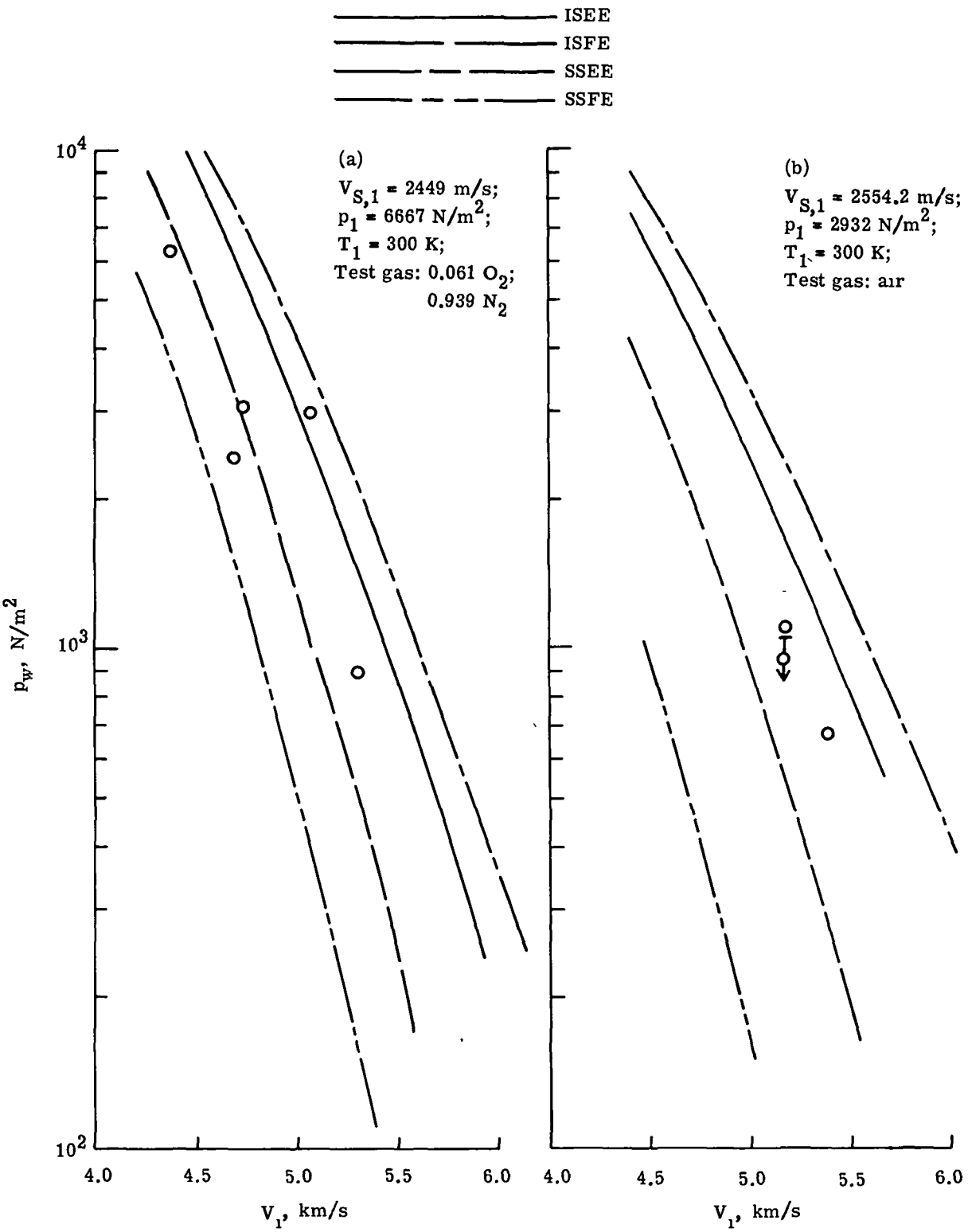

Figure 11.- Comparison of measured and calculated wall pressure.

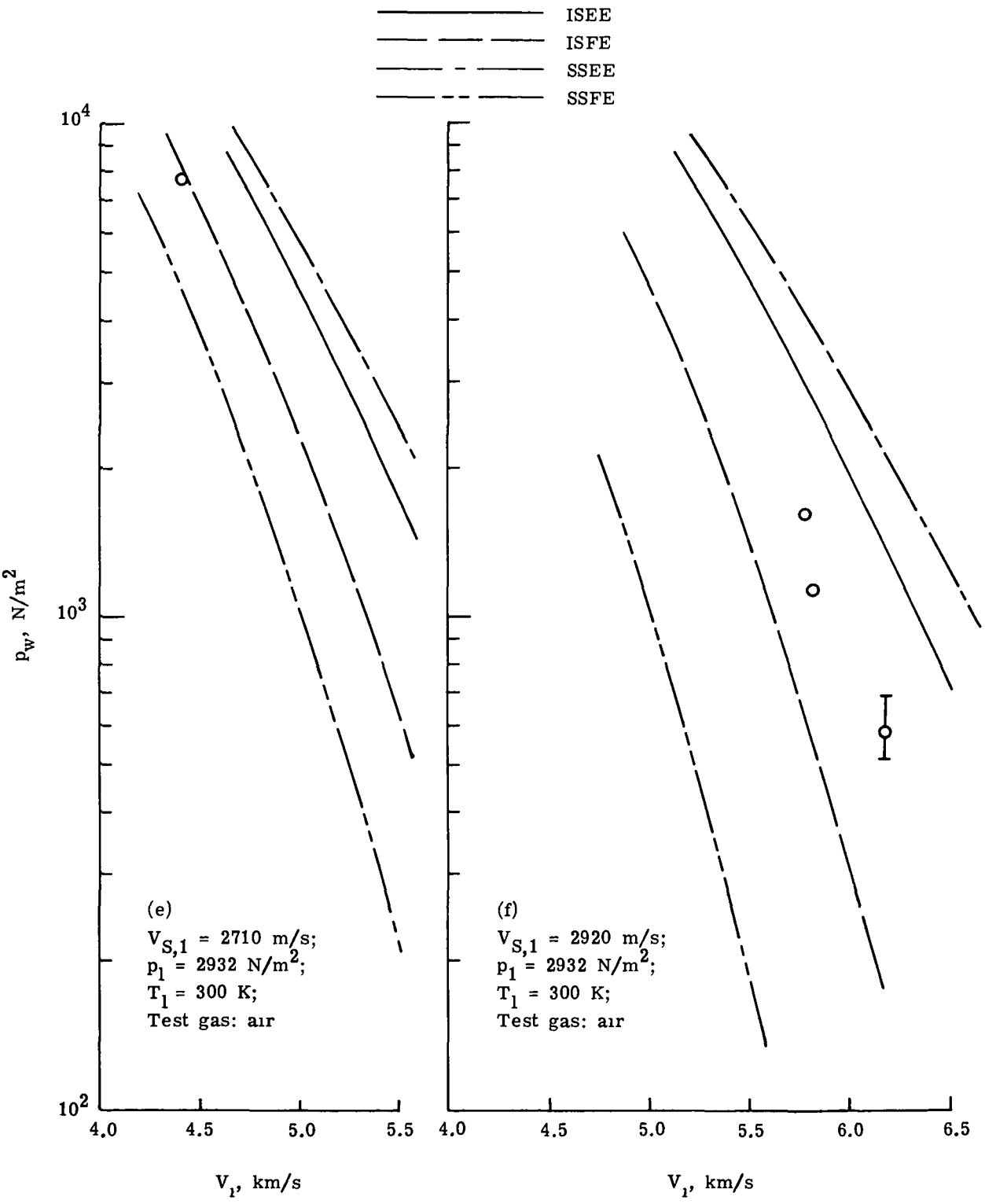

Figure 11.- Concluded.

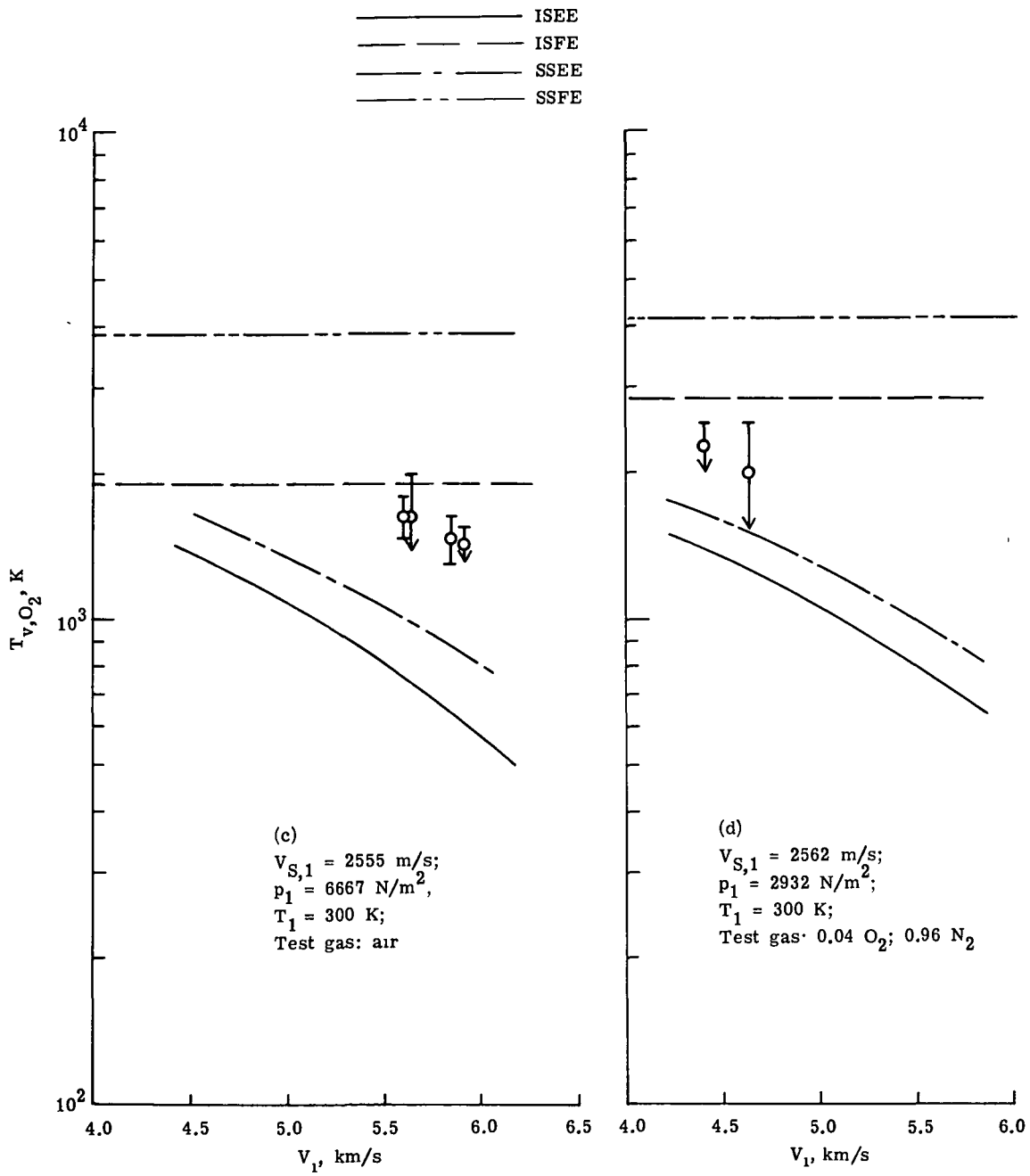

Figure 12.- Continued.

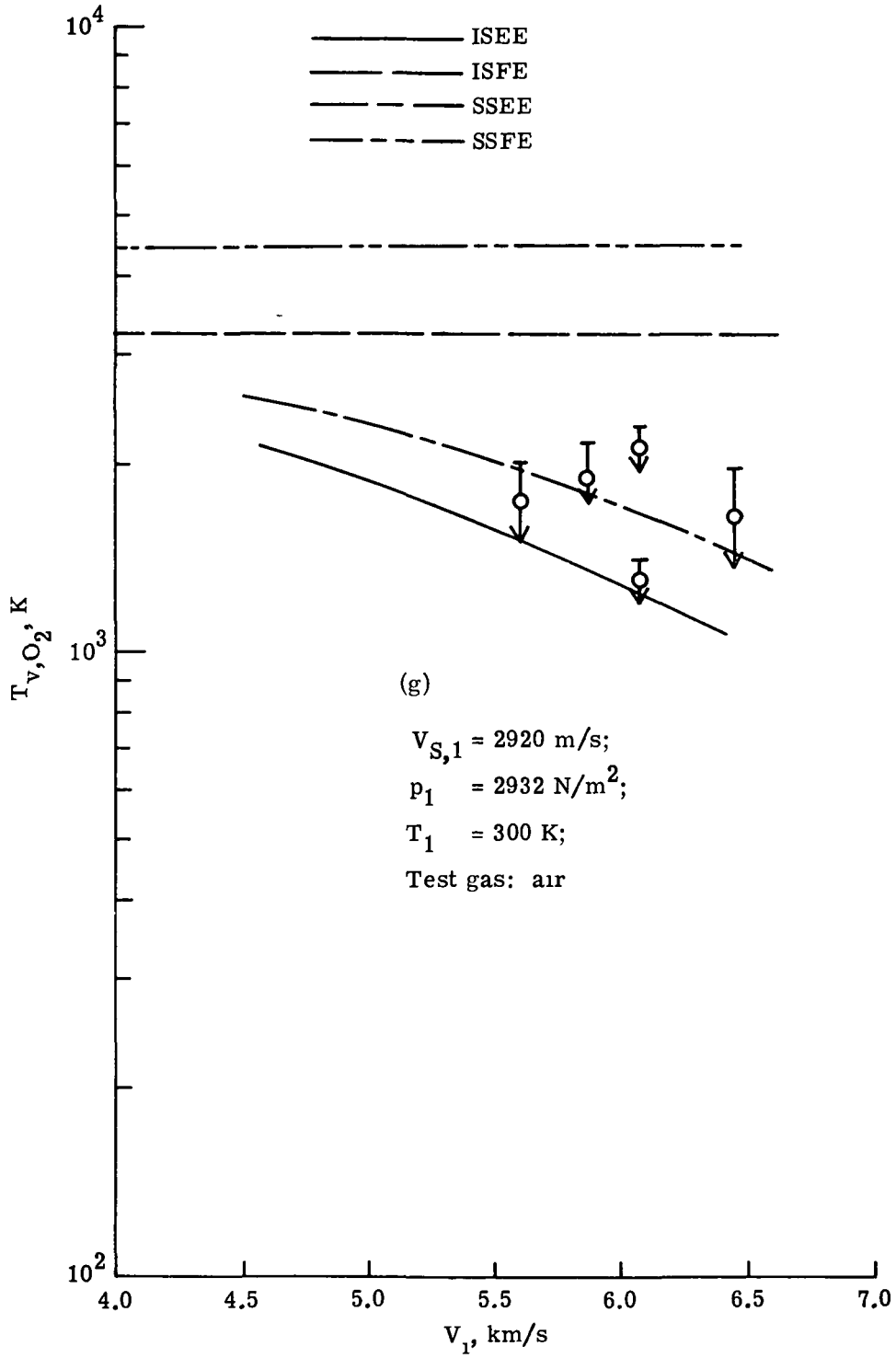

Figure 12.- Concluded.

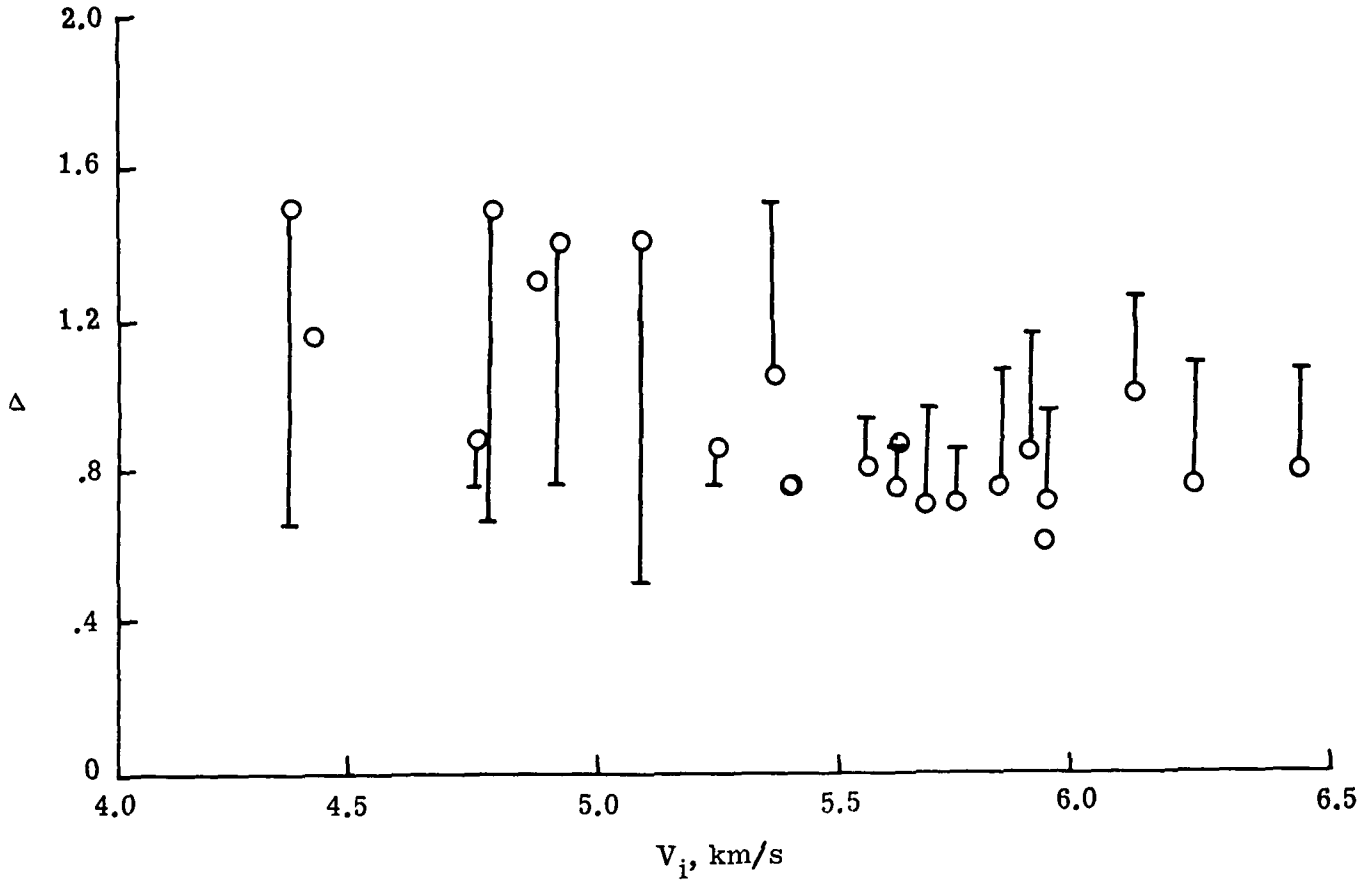

Figure 14.- Variation of Δ with interface velocity and times.

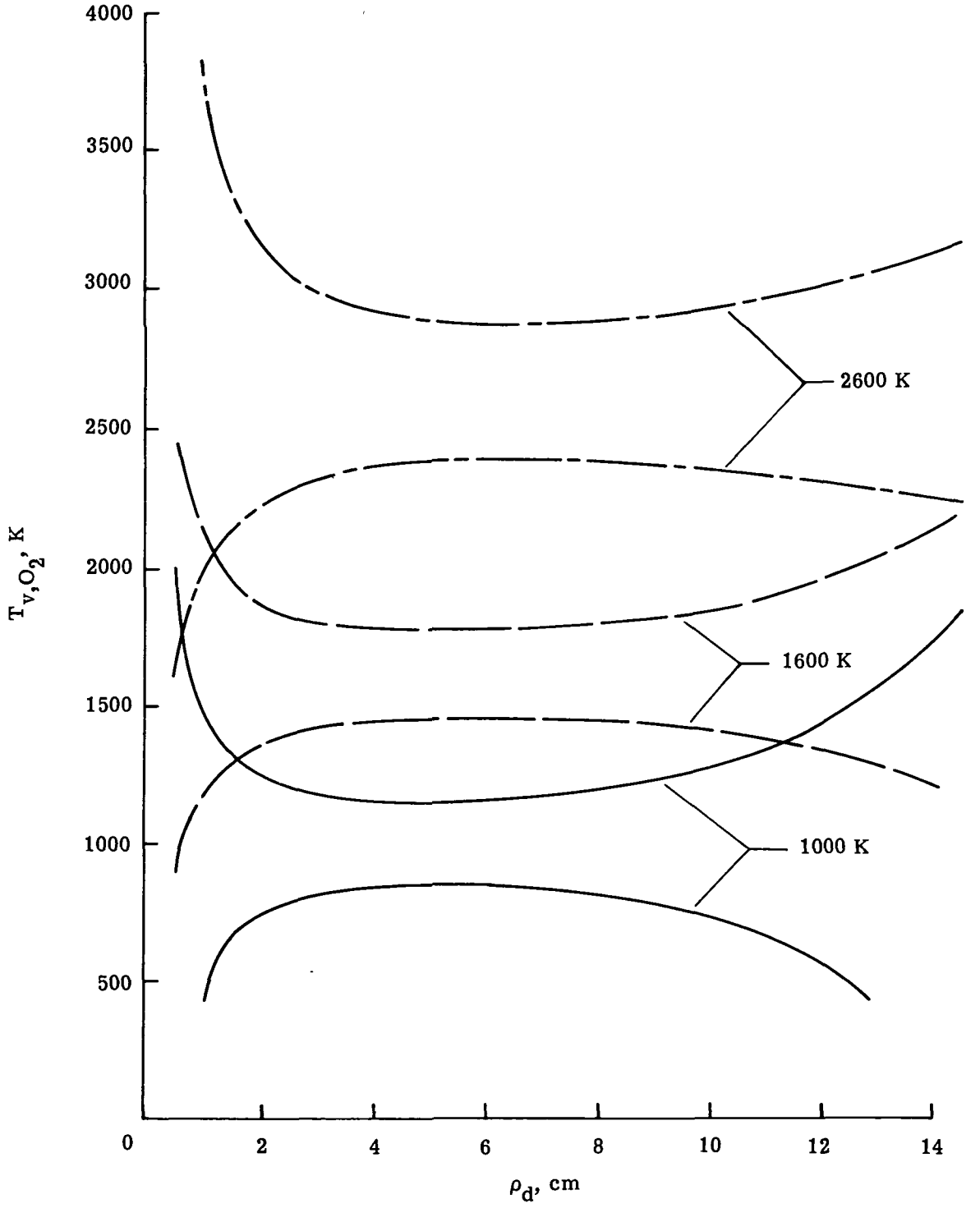

Figure 16.- Temperature error caused by 1 percent measurement error.

NATIONAL AERONAUTICS AND SPACE ADMINISTRATION
WASHINGTON, D C 20546

OFFICIAL BUSINESS
PENALTY FOR PRIVATE USE $300

SPECIAL FOURTH-CLASS RATE BOOK

POSTAGE AND FEES PAID
NATIONAL AERONAUTICS AND SPACE ADMINISTRATION
451

U.S.MAIL

POSTMASTER · If Undeliverable (Section 158 Postal Manual) Do Not Return

"The aeronautical and space activities of the United States shall be conducted so as to contribute . . to the expansion of human knowledge of phenomena in the atmosphere and space The Administration shall provide for the widest practicable and appropriate dissemination of information concerning its activities and the results thereof."

—NATIONAL AERONAUTICS AND SPACE ACT OF 1958

NASA SCIENTIFIC AND TECHNICAL PUBLICATIONS

TECHNICAL REPORTS Scientific and technical information considered important, complete, and a lasting contribution to existing knowledge.

TECHNICAL NOTES Information less broad in scope but nevertheless of importance as a contribution to existing knowledge.

TECHNICAL MEMORANDUMS Information receiving limited distribution because of preliminary data, security classification, or other reasons Also includes conference proceedings with either limited or unlimited distribution.

CONTRACTOR REPORTS Scientific and technical information generated under a NASA contract or grant and considered an important contribution to existing knowledge.

TECHNICAL TRANSLATIONS Information published in a foreign language considered to merit NASA distribution in English

SPECIAL PUBLICATIONS Information derived from or of value to NASA activities. Publications include final reports of major projects, monographs, data compilations, handbooks, sourcebooks, and special bibliographies

TECHNOLOGY UTILIZATION PUBLICATIONS Information on technology used by NASA that may be of particular interest in commercial and other non-aerospace applications. Publications include Tech Briefs, Technology Utilization Reports and Technology Surveys.

Details on the availability of these publications may be obtained from:

SCIENTIFIC AND TECHNICAL INFORMATION OFFICE

NATIONAL AERONAUTICS AND SPACE ADMINISTRATION

Washington, D.C. 20546